Probing and Controlling the Bonds of an Artificial Molecule

Alexander W. Holleitner,[1]* Robert H. Blick,[1] Andreas K. Hüttel,[1] Karl Eberl,[2] Jörg P. Kotthaus[1]

We demonstrate how molecular quantum states of coupled semiconductor quantum dots are coherently probed and manipulated in transport experiments. The applied method probes quantum states by the virtual cotunneling of two electrons and hence resolves the sequences of molecular states simultaneously. This result is achieved by weakly probing the quantum system through parallel contacts to its constituting quantum dots. The overlap of the dots' wave functions and, in turn, the splitting of molecular states are adjusted by the direct influence of coupling electrodes.

Coupled quantum dots in semiconductor materials are often referred to as artificial molecules, because these electron boxes allow us to precisely control the number of charge carriers and their mutual interaction (*1*, *2*). For future quantum information processing, entangled quantum states within such mesoscopic systems need to be implemented in electronic circuits (*3*, *4*). This requires precise control of the bonds of the artificial molecule in situ. In this context, coupled dots can be used for investigating the probing mechanism of quantum physics; that is, how to attach leads to real molecules. Generally the interaction of quantum systems with their environment induces decoherence and the decay of quantum superpositions (*5*). Key questions are how accurately the coupling of two artificial atoms can be adjusted and how coherent coupling can be monitored noninvasively without destroying the molecular quantum states. It has already been shown in transport (*6*, *7*) and microwave (*8*, *9*) spectroscopy that the transition from ionic to covalent binding in quantum dot molecules can be traced. The detection mechanism for those techniques relies on the transmission of a single electron through the coupled dot system. In contrast, we use a cotunneling mechanism involving two electrons tunneling, simultaneously, to probe the coupling between the dots (*10*). Even though the probed quantum states are only weakly coupled to adjacent reservoirs, the dynamics resemble the Kondo effect (*11*–*16*), in which hybridization of electron states with source and drain contacts is desired.

The experimental setup is diagramed in Fig. 1A. As for real molecules, two valence electrons are exchanged between both quantum dots (purple double arrow). This two-electron state couples to individual source and drain contacts by tunneling barriers (black double arrows). The tips of the Schottky gates (Fig. 1B) form two small quantum dots (indicated by blue circles), each containing about 20 electrons. The overlap of the dot wave functions can be tuned by the tunneling barrier, set by voltages on gates A and B (white). In order to complete the setup of Fig. 1A, the source and drain contact regions of both dots (dashed lines) are patterned by an additional resist layer (*7*) (beige). This layer prevents depletion of the electron gas below gates A and B, and electrons eventually tunnel through dot 1 and dot 2. The parallel access to the two dots enables correlated tunneling of two valence electrons simultaneously. This phenomenon is shown in Fig. 1C: (i) The left diagram shows only a single valence electron in the dots connected to the reservoirs through the tunneling processes (double arrow). The valence is indicated by a single line connecting the dots. (ii) The identical case is depicted where the valence electron connects to the reservoirs via dot 2. (iii) The situation we are investigating is characterized by a valence number of two, represented by two lines; here, both covalent

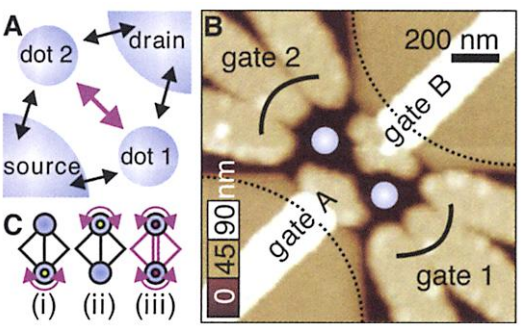

Fig. 1. (**A**) Experimental layout. An artificial molecule is formed out of two quantum dots within a two-dimensional electron gas 90 nm below the surface of an aluminum gallium arsenide/gallium arsenide heterostructure. Valence electrons are exchanged between both dots (purple double arrow) and are detected by measuring the system's conductance through cotunneling events. Electrons tunnel via both dots from source to drain (black double arrows) (*7*). (**B**) Atomic force microscopy picture of the sample. The heights are color coded as indicated on the lower left lateral scale. In order to define the two quantum dots (sketched as two blue circles), negative voltages are applied to Schottky gates A, B, 1, and 2, made from gold (bright beige and white). The electron gas, with a sheet density of about $n_s = 1.7 \times 10^{15}$ m^{-2} and an electron mobility (μ) of 80 m^2/Vs at 4.2 K, is partially depleted and forms two quantum dots with roughly 20 electrons each. Both quantum dots are equally connected to drain and source contacts, as is essential for the presented spectroscopy. (**C**) Sketches of the characteristic electronic configurations within the dots.

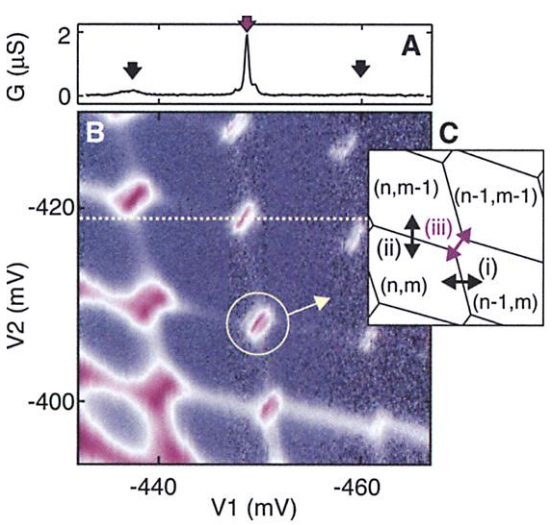

Fig. 2. (**A**) Differential conductance trace G_{SD} at a small ac voltage $V_{SD} = 10$ μV versus voltage $V1$ at gate 1 ($T_{bath} = 40$ mK). (**B**) Charging diagram of the double quantum dot obtained by additionally sweeping voltage $V2$ at gate 2 (displayed in a logarithmic color representation). Addition energies (E) of both dots are found to be $E_1 = e^2/C = 2.22$ meV (where C is capacity) and $E_2 = 2.76$ meV with single particle levels of $\varepsilon \cong 240$ μeV. (**C**) Charge configurations of the encircled resonance of 2(B) are sketched by brackets (n,m) with n electrons on dot 1 and m electrons on dot 2.

[1]Center for NanoScience and Sektion Physik, Ludwig-Maximilians-Universität, Geschwister-Scholl-Platz 1, 80539 München, Germany. [2]Max-Planck-Institut für Festkörperforschung, Heisenbergstrasse 1, 70569 Stuttgart, Germany.

*To whom correspondence should be addressed. E-mail: Alex.Holleitner@physik.uni-muenchen.de

dimer states are occupied and equally coupled to source and drain (arrows).

In transport measurements on the coupled dot system (Fig. 2A), a typical line plot of conductance (G) versus gate voltage ($V1$) detected in standard lockin technique is shown. The maximum conductance level of $G \approx 0.1\ e^2/h$ (where e is electron) indicates the weak coupling of the dots to the leads. The data were taken in a dilution refrigerator with 40 mK bath temperature at an ac voltage of $V_{SD} = 10\ \mu V$. Although high tunneling barriers to the leads strongly suppress the conductance for Coulomb blockade resonances for each dot (*17*) (black arrows), we find enhanced transmission at certain gate voltages (purple arrow). More information is gained by tracing the resonances in a charging diagram (Fig. 2B). The data trace of Fig. 2A is represented by the dashed line at $V2 \sim -420$ mV. The sets (n,m) are diagrammed in Fig. 2C, with the charge configuration with n electrons on dot 1 and m electrons on dot 2 around the encircled resonance. This set is altered by exactly one electron when the border between the hexagons is crossed, so by following route (i) we get from (n,m) to $(n-1,m)$. On resonance, this corresponds to one electron coupling the two dots (left diagram in Fig. 1C). The same is true for route (ii) representing the transition (n,m) to $(n,m-1)$. In route (iii) we observe the effect of central interest here: the coupling of state (n,m) to $(n-1,m-1)$. The simultaneous exchange of two electrons is the main difference from earlier measurements (*7*, *18*) with only one source and one drain contact on coupled dots, where only a single valence electron can be monitored. Hence, the pattern obtained in the present measurements shows the difference in revealing a pronounced resonance for the exchange of two electrons. This behavior is found not only at the crossing point marked but also for all other resonances at corresponding phase boundaries (iii).

Furthermore, the amplitudes of the resonances exceed conventional Coulomb blockade oscillations by up to two orders of magnitude (*19*), and these resonance lines break up, revealing a substructure (already evident in Fig. 2A). This substructure is better resolved in the logarithmic conductance plot versus voltage ($V1$) (Fig. 3A) depicting the encircled resonances of Fig. 2B. As expected for resonant tunneling, the conductance is given by Lorentzians (*17*) (black and dashed lines). The full widths at half maximum (FWHMs) of these resonances decrease linearly with decreasing temperature and show no saturation down to lowest bath temperatures (T_{bath}) of 40 mK (squares in Fig. 3B). This is clear evidence for the dominance of cotunneling (*10*); that is, only two electrons are allowed to tunnel simultaneously at the very same energy (*20*). Consequently, the FWHMs of these cotunnel events are only governed by lifetime broadening of the quantum states involved and inelastic phonon scattering (*21*). In contrast, the FWHMs of conventional Coulomb blockade oscillations (triangles) saturate at about 120 ± 20 mK (arrow in Fig. 3B) (data taken off resonance). The latter reflects saturation of the electron temperature in the source and drain leads commonly caused by radio frequency noise in the supply lines of the setup (*22*). Complementing the coherent two-electron picture, the amplitude of the maximum peak decreases logarithmically with increasing temperature (*23*, *24*) (squares in Fig. 3C). The logarithmic dependence indicates the relation to the Kondo effect (*11*–*16*), even though here the quantum states are only weakly coupled to the leads. Furthermore, a thermally broadened Fermi-Dirac distribution in the source and drain leads allows cotunnel processes through higher energy states within the double dot. First, this result can be seen in the temperature dependence of the amplitude of the side peaks, because the amplitude rises after a certain decrease (circles in Fig. 3, A and C). Second, additional resonances emanate at higher temperatures as discussed below.

Cotunneling of two electrons occupies quantum states of the double quantum dot virtually, without paying Coulomb charging energy (*10*). We demonstrate how these higher order tunneling processes can be applied for noninvasively probing covalent states of the dimer dot. At a T_{bath} of 815 mK, not only triplets (as in Fig. 3A) are found but also a sequence of resonances, as seen in the charging diagram of Fig. 4A (compare to Fig. 2B). The single trace, indicated by a dashed line, is plotted in Fig. 4B including calibration (*25*).

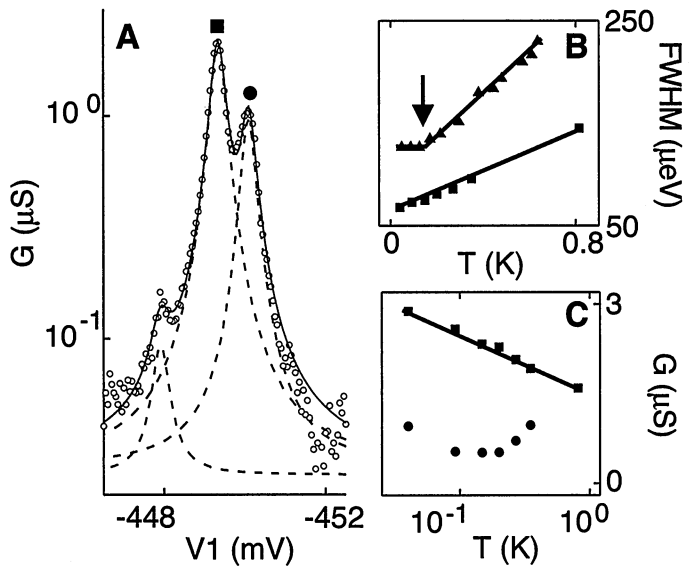

Fig. 3. (**A**) Logarithmic conductance trace of resonant cotunneling (corresponds to encircled resonance in Fig. 2B). (**B**) The FWHMs of cotunneling events are determined only by lifetime broadening of the involved quantum states and decrease linearly with decreasing temperature (squares). In contrast, the FWHMs of typical Coulomb blockade peaks (triangles) are additionally broadened by the Fermi-Dirac energy distribution in the source and drain contacts, which shows a saturation at T_{bath} of 120 ± 20 mK (black arrow) (*7*). (**C**) The amplitude of the center peak [squares in (A) and (C)] decreases logarithmically with increasing temperature, which indicates coherent tunneling of two electrons (*23*, *24*). Circles denote the temperature dependence of the side peak in (A).

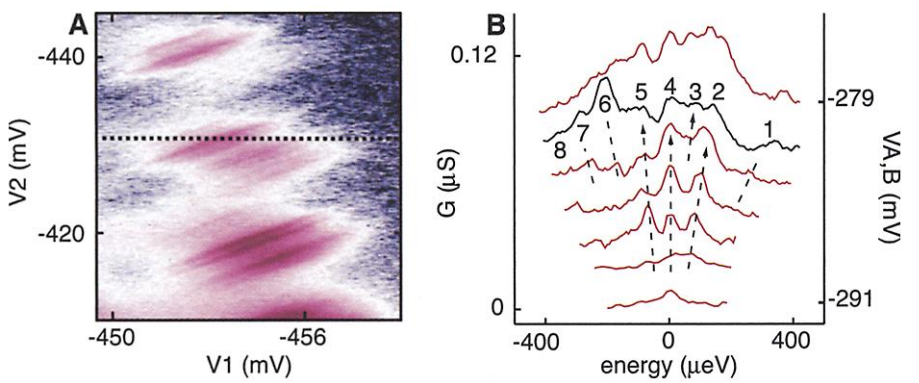

Fig. 4. (**A**) Sequences of covalent molecular states at 815 mK traced by cotunneling of the two binding electrons in the charging diagram. (**B**) The resonances 1 through 8 correspond to the dotted line in Fig. 4A. Increasing the negative voltages applied to gates A and B from –279 mV to –291 mV in steps of 2 mV raises the interdot tunneling barrier, which in turn suppresses all resonances but peak 4. The data are presented with an offset for better visibility.

Eight resonances can be resolved for this interdot tuning with an energy offset ($\Delta\varepsilon$) of about 70 to 120 μeV. Raising the interdot tunneling barrier reduces $\Delta\varepsilon$ (dashed lines), and consequently the number of resonances diminishes to one. As for real dimers, this can be understood by the reduced overlap of the dot wave functions that determines $\Delta\varepsilon$ of corresponding molecular states. The remaining peak is a degenerate multiplet, which unfolds into resonances 2, 3, 4, and 5 as the overlap of two dots' wave functions is increased (indicated by the dashed arrows in Fig. 4B). Furthermore, the energy splitting found is of the same order of magnitude as the one for bonding and antibonding states in coupled dots with one valence electron (*7*). However, here we coherently probe and thus resolve a whole sequence of molecular states.

References and Notes

1. M. Kastner, *Phys. Today* **46** (no. 1), 24 (1993).
2. C. Livermore, C. H. Crouch, R. M. Westervelt, K. L. Campman, A. C. Gossard, *Science* **274**, 1332 (1996).
3. M. Bayer *et al.*, *Science* **291**, 451 (2001).
4. M. N. Leuenberger, D. Loss, *Nature* **410**, 789 (2001).
5. C. J. Myatt *et al.*, *Nature* **403**, 269 (2000).
6. R. H. Blick, D. Pfannkuche, R. J. Haug, K. von Klitzing, K. Eberl, *Phys. Rev. Lett.* **80**, 4032 (1998).
7. A. W. Holleitner, C. R. Decker, H. Qin, K. Eberl, R. H. Blick, *Phys. Rev. Lett.* **87**, e256802 (2001).
8. T. H. Oosterkamp *et al.*, *Nature* **395**, 873 (1998).
9. H. Qin, A. W. Holleitner, K. Eberl, R. H. Blick, *Phys. Rev. B* **64**, R241302 (2001).
10. D. W. Averin, Y. V. Nazarov, in *Single Charge Tunneling*, H. Grabert, M. H. Devoret, Eds., vol. 294 of *NATO ASI Series B* (Plenum, New York, 1992), pp. 217–247.
11. D. Goldhaber-Gordon, H. Shtrikman, D. Mahalu, D. Abusch-Magder, U. Meirav, *Nature* **391**, 156 (1998).
12. S. M. Cronenwett, T. J. Oosterkamp, L. P. Kouwenhoven, *Science* **281**, 540 (1998).
13. F. Simmel, R. H. Blick, J. P. Kotthaus, W. Wegscheider, M. Bichler, *Phys. Rev. Lett.* **83**, 804 (1999).
14. J. Schmid, J. Weis, K. Eberl, K. von Klitzing, *Phys. Rev. Lett.* **84**, 5824 (2000).
15. H. Jeong, A. Chang, M. R. Melloch, *Science* **293**, 2221 (2001).
16. C. A. Büsser, E. V. Anda, A. L. Lima, M. A. Davidovich, G. Chiappe, *Phys. Rev. B* **62**, 9907 (2000).
17. C. W. J. Beenakker, *Phys. Rev. B* **44**, 1646 (1991).
18. F. Hofmann *et al.*, *Phys. Rev. B* **51**, 13872 (1995).
19. Conventional Coulomb blockade oscillations are found to be below the average noise level of $\delta G \leq 0.03$ μS.
20. Fermi's golden rule: The rate of cotunnel events is independent of temperature and only given by $\Gamma = 2\pi/\hbar\Sigma|A|\delta(\varepsilon_1 - \varepsilon_2)$, with $\hbar$, Planck's constant divided by 2π, A as amplitude, and a vanishing energy difference between levels ε_1 and ε_2.
21. T. Fujisawa *et al.*, *Science* **282**, 932 (1998).
22. The filter boxes in the setup are all integrated at room temperature.
23. D. Goldhaber-Gordon *et al.*, *Phys. Rev. Lett.* **81**, 5225 (1998).
24. Underlying conventional Coulomb blockade oscillations start to take over only above $T_{Bath} = 1.2$ K.
25. For energy calibration, from nonlinear transport spectroscopy on each dot individually we find the energy/voltage ratio of each gate and dot to be $\alpha(V_1,\mathrm{dot}_1) = 0.138$ and $\alpha(V_2,\mathrm{dot}_2) = 0.15$.

26. We thank J. v. Delft and F. Wilhelm for stimulating discussions. Supported by the Deutsche Forschungsgemeinschaft, the Bundesministerium für Forschung und Technologie, and the Defense Advanced Research Projects Agency.

25 February 2002; accepted 14 May 2002

Sequence-Specific Molecular Lithography on Single DNA Molecules

Kinneret Keren,[1] Michael Krueger,[1] Rachel Gilad,[1] Gdalyahu Ben-Yoseph,[1,2] Uri Sivan,[1,2] Erez Braun[1,2]*

Recent advances in the realization of individual molecular-scale electronic devices emphasize the need for novel tools and concepts capable of assembling such devices into large-scale functional circuits. We demonstrated sequence-specific molecular lithography on substrate DNA molecules by harnessing homologous recombination by RecA protein. In a sequence-specific manner, we patterned the coating of DNA with metal, localized labeled molecular objects and grew metal islands on specific sites along the DNA substrate, and generated molecularly accurate stable DNA junctions for patterning the DNA substrate connectivity. In our molecular lithography, the information encoded in the DNA molecules replaces the masks used in conventional microelectronics, and the RecA protein serves as the resist. The molecular lithography works with high resolution over a broad range of length scales from nanometers to many micrometers.

Recent advances in the realization of molecular-scale devices (*1*, *2*) highlight their integration into functional circuits as a major challenge. Successful attempts toward this goal include the use of e-beam lithography for wiring carbon nanotubes to form logic circuits (*3*) and the construction of logic gates from nanowire building blocks aligned by flow (*4*).

An alternative route to nanometer-scale electronics relies on molecular recognition and self-assembly. In such a bottom-to-top approach, the information is encoded into the components, which then self-assemble according to that information to form the structure. DNA-programmed assembly is a particularly promising strategy [see, for example, (*5*–*9*)]. We have previously shown that DNA molecules can be uniformly coated with metal to form thin metallic conductive wires that can be attached to macroscopic electrodes by virtue of the DNA molecular recognition properties (*8*, *9*). Molecular electronics, however, requires more elaborate manipulations, including the formation of richer geometries, wire patterning at molecular resolutions, and molecularly accurate device localization. In

[1]Department of Physics, [2]Solid State Institute, Technion-Israel Institute of Technology, Haifa 32000, Israel.

*To whom correspondence should be addressed. E-mail: erez@physics.technion.ac.il

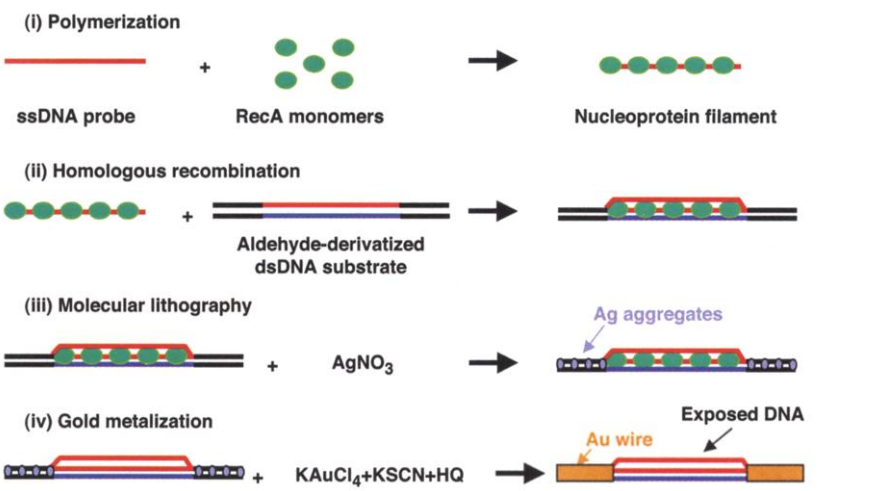

Fig. 1. Schematics of the homologous recombination reaction and molecular lithography. In part (i), RecA monomers polymerize on a ssDNA probe molecule to form a nucleoprotein filament. In part (ii), the nucleoprotein filament binds to an aldehyde-derivatized dsDNA substrate molecule at a homologous sequence. In part (iii), incubation in $AgNO_3$ solution results in the formation of Ag aggregates along the substrate molecule at regions unprotected by RecA. In part (iv), the Ag aggregates serve as catalysts for specific gold deposition, converting the unprotected regions to conductive gold wires. HQ, hydroquinone.